Article

Broadband Dielectric Spectroscopic Detection of Ethanol: A Side-by-Side Comparison of ZnO and HKUST-1 MOFs as Sensing Media †

Papa K. Amoah [1,2], Zeinab Mohammed Hassan [3], Pengtao Lin [1,2], Engelbert Redel [2], Helmut Baumgart [1,2] and Yaw S. Obeng [4,*]

1 Department of Electrical and Computer Engineering, Old Dominion University, Norfolk, VA 23529, USA; pamoa001@odu.edu (P.K.A.); pxlin002@odu.edu (P.L.); hbaumgar@odu.edu (H.B.)
2 Applied Research Center at Thomas Jefferson National Accelerator Laboratories, 12050 Jefferson Avenue, Suite 721, Newport News, VA 23606, USA
3 Karlsruhe Institute of Technology, Institute of Functional Interfaces (IFG), Hermann-von-Helmholtz-Platz 1, 76344 Eggenstein-Leopoldshafen, Germany; zeinab.hassan@kit.edu (Z.M.H.); engelbert.redel@partner.kit.edu (E.R.)
4 Physical Measurement Laboratory, National Institute of Standards and Technology, 100 Bureau Drive, Gaithersburg, MD 20899, USA
* Correspondence: yaw.obeng@nist.gov
† Certain commercial equipment, instruments, or materials are identified in this paper in order to specify the experimental procedure adequately. Such identification is not intended to imply recommendation or endorsement by the National Institute of Standards and Technology, nor is it intended to imply that the materials or equipment identified are necessarily the best available for the purpose. Contribution of the National Institute of Standards and Technology, not subject to copyright.

Abstract: The most common gas sensors are based on chemically induced changes in electrical resistivity and necessarily involve making imperfect electrical contacts to the sensing materials, which introduce errors into the measurements. We leverage thermal- and chemical-induced changes in microwave propagation characteristics (i.e., S-parameters) to compare ZnO and surface-anchored metal–organic-framework (HKUST-1 MOF) thin films as sensing materials for detecting ethanol vapor, a typical volatile organic compound (VOC), at low temperatures. We show that the microwave propagation technique can detect ethanol at relatively low temperatures (<100 °C), and afford new mechanistic insights that are inaccessible with the traditional dc-resistance-based measurements. In addition, the metrological technique avoids the inimical measurand distortions due to parasitic electrical effects inherent in the conductometric volatile organic compound detection.

Keywords: broadband dielectric microwave spectroscopy; solid-state ZnO-sensing material; HKUST-1 metal–organic framework (MOF) sensing material; ethanol detection

1. Introduction

1.1. Volatile Organic Compound (VOC) Detection

Intrinsic material property changes due to analyte adsorption and reactions of the sensing materials are the basis of many conductometric chemical sensors [1–3]. In gas sensing applications, most of the sensing materials tend to be metal oxides (MO, mostly II-VI semiconductors) due to their low cost, simple design and ease of production, short response time, wide detection range, and resistance to harsh working environments [4]. For these chemical sensors to be successful, there must be (i) charge transfer between the analyte and the sensing materials, and (ii) a reversible analyte concentration dependence of the measurand [5]. Along these lines, there is a need for effective and efficient methods to monitor volatile organic compounds (VOCs). Highly sensitive analytical chemistry techniques, such as spectrophotometry, fluorometry, gas chromatography (GC), and high-performance liquid chromatography (HPLC) have been used for the accurate quantification

of VOCs. However, these techniques are expensive, bulky, have low throughput, require time-consuming pretreatment steps and highly skilled operators, consume substantial amounts of power, and do not provide real-time information for risk mitigations and decision making [6]. These limitations preclude most of the current VOC detection techniques from being used in the internet of things (IoT, internet edge) applications.

For IoT applications, the sensor should be small, inexpensive, and fast, with high sensitivity, selectivity, and stability for specific applications [7–9]. Emerging 2D material, such as graphene, graphene oxide, phospherene, and transition metal dichalcogenides (e.g., MoS_2), together with carbon nanotubes (CNTs), are being cointegrated with digital devices into viable gas sensors, mostly as chemically sensitive resistors (chemoresistors), chemically sensitive field-effect transistors (chemFETs), or carbon nanotube field-effect transistors (CNTFETs). For example, MoS_2 chemoresistors have been shown to be sensitive to different organic compounds including triethylamine (TEA) and acetone, with detection limits as low as 0.16 parts per trillion for nitric oxide gas molecules. In addition to changing the channel resistance, analyte-specific changes to the low frequency $1/f$ noise spectra of graphene chemFETs may be used as a VOC detection measurand in these chemFETs [10]. The selectivity and sensitivity of 2D-material sensors can be tuned with chemical functionalization of the surface of the sensing material. These devices can be further optimized with device gate bias adjustments to electrostatically change the carrier concentration in the channel to an optimal point [10]. Advances in heterogeneous integration schemes are leveraging these emerging materials into three dimensional (3D) sensor design for IoT applications; for example, a single chip CNTFET nanosystem that senses, stores the data, and classifies ambient gases has been demonstrated [11].

Unfortunately, many of these chemFETs and chemoresistors require energy-intensive internal heating for optimal operation [12]. For IoT and autonomous applications, new metrology that does not require high temperature for transduction, such as analyte-induced volume and surface capacitance, are needed [12]. Metal–organic frameworks (MOFs) have emerged as a novel class of tunable electronic nanomaterials; they combine the advantages of long-range order of inorganic conductors with the synthetic flexibility of organic semiconductors [13]. These MOFs have the potential to overcome many of the challenges of selectivity that limit other sensor materials, which depend on charge-transfer processes to change resistivity [14,15]. Altering band structures in MOF-based sensors from analyte surface reactions is possible, similar to those in metal-oxide semiconductors [5,16]. The ultralarge surface areas, high porosity, and the ability to form coordination complex, clathrates-like structures with analyte molecules make MOFs attractive for selective gas sensing [17]. Furthermore, many of these MOF-based gas sensors work at room temperature, negating the need for heating [12,17].

In addition, the resistivity measurements of the chemoresistor-based sensors necessarily involve making electrical contacts to the sensing materials. This can introduce non-negligible contact impedance in series with the sensing materials, especially in the two-pole measurement techniques often used with the coulometric gas sensors. In such systems, the errors from the connecting cables can be significant, especially when the resistance of the sample is lower than approximately 50 Ω [18]. Noncontact microwave gas sensing is emerging as an alternative to coulometric gas sensing; a microwave resonant cavity technique has also been used to detect and to distinguish between methanol, ethanol, and acetone in the 0–200 ppm range at room temperature [19]. Capacitive sensing of VOCs, with a dielectric layer consisting of compacted Cu-BTC nanoparticles, has also been demonstrated [17]. However, the performance metrics of these microwave gas sensors, such as selectivity, sensitivity, reproducibility, and long-term stability, are currently not yet well established. Furthermore, the impact of environmental factors such as temperature and humidity are currently not well understood [20]. Thus, there is a need to improve our fundamental knowledge of microwave gas sensors.

The mechanisms involved in chemoresistive gas sensing are not well understood. For example, while transduction in the metal oxides are temperature dependent, the mech-

anisms behind the temperature dependence are not well understood [21]. Similarly, the mechanisms underpinning MOF-based gas sensing are currently not fully understood [12]; presumably, the analyte molecules oxidize when they contact the sensing materials [14]. In traditional conductometric sensing, the redox reactions convert analyte–sensor interactions into measurable dc resistance through changes in electrical resistivity because of electron injection into, or withdrawal of electrons from, the electronic conduction band structure of the sensing element [22,23]. In this regard, the electrically active defects in the MOF materials appear to behave similar to those in semiconducting metal oxides [16]. Here, we compare low-temperature sensing of ethanol on substrate-anchored ZnO nanorods and TCNQ-doped HKUST-1 MOF, through microwave impedance changes, to gain mechanistic insights into the microwave sensing of ethanol vapor. The TCNQ-doped HKUST-1 SURMOF provides a well-characterized platform for such investigations [24]. We have shown elsewhere that the thermal conductivities of SURMOF films are commensurate with their single crystalline MOF analogues, and decrease in the presence of adsorbates [25], owing to increased vibrational scattering introduced by extrinsic guest–MOF collisions, and guest-molecule-induced hybridization of low-frequency modes [26]. We have also demonstrated elsewhere that, in contrast to the traditional coulometric techniques, ZnO nanotubes can sense ethanol at temperatures under 100 °C by using broadband microwave dielectric spectroscopy (BDS) [27].

1.2. Broadband Dielectric Spectroscopy (BDS) Background

Accumulation and alignment of charged defects play significant roles in VOC detection, as their state changes in the presence of reactive organic molecules. When exposed to electromagnetic waves, the dipolar defects oscillate to keep up with the rapidly changing external electric fields; at some critical frequency the polarizability cannot keep up with the velocity of the applied fields, resulting in dielectric loss. The displacement of the bound charges in the sensing media in an external electric field, E, results in a dipolar moment, m, and a torque, G, as the dipolar moment orientates parallel to the electric field in opposition to the applied field. This produces a net polarization of the material which determines the dielectric response of materials to electromagnetic radiation. In isotropic media, the volume density of polarization is directly proportional to the applied electric field intensity [28]. Thus, fundamentally, the elementary processes that underpin VOC detection with metal oxides involve changes in polarizability, and the resultant changes in electrical characteristics, of the sensing media. These changes alter the propagation characteristics of radio frequency or microwaves in such media and instigate microwave absorption / energy dissipation. We define a complex dielectric function that measures the electric displacement field due to the presence of an electric field in a dielectric material, as given in Equation (1)

$$\varepsilon(\omega) = \varepsilon 1(\omega) + i\varepsilon 2(\omega) \tag{1}$$

where $\omega = 2c\pi/\lambda$ is the frequency, c is the speed of light, and λ is the wavelength; $\varepsilon 1(\omega)$ describes how much the material is polarized when an electric field is applied, and $\varepsilon 2(\omega)$ is related to the absorption of the material [29,30]. The dielectric polarizability at high frequencies sets the scale for radiation absorption, while at low frequencies it determines the nonlinear effects.

When electromagnetic waves interact with matter, the incident microwave signal scatters according to the material's permittivity. During the signal scattering, a portion of the radiation is transmitted through the sample while the remainder is reflected toward the source, as described by Snell's law [28]. The ratio of transmitted to reflected energies depends in part on the impedance mismatch between the material under test (MUT) and the source. The signal scattering from the electrical interfaces is summarized as a matrix of S-parameters that quantifies how RF energy propagates through a multiport network such as a vector network analyzer (VNA). The S-parameters can be extracted in the frequency domain (FD), time domain (TD), or hybrid modes based on the form of the interrogating signal [31]. In this work, we used a two-port hybrid technique, in which the input excitation

is convolved with the transfer function of the sensor (h(f)) loaded with the MUT. A typical two-port measurement contains four S-parameters (S11, S21, S12, and S22), which are vector quantities representing the magnitude and the phase of the frequency-dependent characteristics of the MUT. A portion of the incident wave is transmitted (i.e., S21 and S12) or reflected (S11 and S22). The portion of the transmitted signal exits the MUT with different magnitude and phase from the incident signal; thus, S21 and S12 also encode the phase difference between a transmitted signal and an incident signal. The S-parameters can be analytically transformed to produce the characteristic circuit element of the analyte, as described elsewhere [32]. Broadband microwave dielectric spectroscopy (BDS) measures the dispersive and dissipative dielectric behavior of the analyte as a function of frequency, i.e., changes in the polarizability of the analyte. Because input excitation is convoluted by the transfer function of the sensor loaded with the MUT, i.e., (h(f)), to generate the output S-parameter, the BDS has the advantage of rapidly interrogating a dynamic range of material characteristics [33]. Polar functional groups in organic molecules (e.g., VOCs) are electron-rich and highly polarizable, hence readily absorb microwave energy to distort as the electrons transfer from one stable state to an excited state with higher energy, forming the electron polarization in rapidly changing magnetic fields. Here, by measuring the MW insertion loss characteristics (S21) as a function of the experimental variables, we use the S-parameters to evaluate the chemoinduced changes (CIC) in the VOC adsorbed on the MO-sensing materials. Thus, in this work, the S-parameters are functionals of frequency and experimental stress (i.e., F[h(f)]).

Gas monitoring with microwave-based metrology is well known, but the technology has some performance-limiting gaps. Specifically, performance metrics such as selectivity, sensitivity, reproducibility, and long-term stability are not yet well established, and the impact of environmental factors such as temperature and humidity are currently not well understood [20]. We had previously used microwave-based broadband dielectric spectroscopy (BDS) [34] to investigate the initial stages of ethanol vapor detection with ZnO nanorods [27]. The BDS detection of VOC with semiconductor metal oxides involve changes in polarizability, i.e., the repolarization of the permanent electrical dipoles, which instigates microwave absorption / energy dissipation during the rotation and orientation of the dipoles [34,35]. When microwaves interact with the analyte (i.e., MUT) the incident microwave signal scatters according to the material's permittivity; the signal scattering is a function of frequency and experimental stress (i.e., F[h(f)]). The input excitation is convoluted by the transfer function of the sensor loaded with the MUT, i.e., (h(f)), to generate the output S-parameter [31]. In this paper, using BDS metrology, we compare ethanol vapor sensing on ZnO nanorods and surface-anchored metal–organic-framework thin films (HKUST-1 SURMOF) as sensing materials at temperatures under 100 °C. We have shown elsewhere that surface ZnO nanorods offer significantly increased sensing surfaces that improve the sensitivity and reduce the long response / recovery times [33]. Contactless broadband dielectric spectroscopy (BDS) is most advantageous for monitoring reactions involving some degree of charge transfer regardless of the nature of the charge carriers, i.e., electrons and holes [36]. The microwave signals are absorbed when inserted into such materials due to changes in the polarizability of the MO–adsorbate interface. We use the S-parameters to evaluate the redox behavior of ethanol molecules adsorbed on the sensing materials, by measuring the insertion loss characteristics (S21) as a function of the experimental variables [37,38]. With proper calibration, the S21 amplitude can be correlated to the total impedance of the GSG waveguide and gas-sensing device. Thus, we can use the S21 magnitude as an index to the changes in the MUT in response to an external perturbation, as shown by Equation (2), where Z_Γ and Zo are the instantaneous and characteristic impedances of the device under test, respectively:

$$z_\Gamma = z_0 \frac{2(1 - s_{21})}{s_{21}} \tag{2}$$

2. Experimental

2.1. Sensing Material Preparation

For the ZnO-sensing study, the gas sensor device consisted of hydrothermally synthesized ZnO nanorods grown on a random polycrystalline fine-grain ZnO seed layer, which was fabricated by atomic layer deposition (ALD) on a native-oxide-covered p-type boron-doped silicon substrate with resistivity of about 4 Ωcm to about 6 Ωcm and a thickness of about 500 μm to about 550 μm, as we described previously [39]. The surface-anchored ZnO nanorods used in the ethanol detection are described elsewhere [38]. In our current study, the average ZnO nanorod was ~500 nm tall and ~50 nm in diameter [27]. We note that the ZnO nanorods do not all appear to align perfectly at 90 degrees with respect to the small grains of the ZnO seed layer. Whether the hydrothermal ZnO nanorods all grow at 90 degrees or display some angular variation is immaterial for the gas-sensing reaction; the most important factor is the resulting surface-to-volume ratio.

Polycrystalline HKUST-1 surface-mounted metal–organic framework thin films (SUR-MOFs) were grown by quasi liquid-phase epitaxy (LPE surface-anchored) on plasma activated borosilicate SiO_2 glass, as described elsewhere [40]. In this work, we used $\approx$35 nm thick HKUST-1 films, formed from 30 spray-cycles [41]. The greenish color of our films is indicative of Cu^{2+}/Cu^+ defects [42]. Loading of fresh HKUST-1 MOF thin films is accomplished by infiltration with 7,7,8,8-tetracyano-quinodimethane (TCNQ), as described in the open literature [43]. Planar-view scanning electron micrography (SEM) of the TCNQ-loaded SURMOFs films shows uniform distribution of grain size composed of primarily large grains separated by what appears to be wide cracks between the MOF domains [40]. The cracks are presumably formed as a result of significant unit-cell change when the pristine HKUST-1 is doped with TCNQ [40]. The substrates with the samples were diced into 1.5 cm by 2.5 cm pieces and stored in a pure nitrogen atmosphere prior to use.

Analytical grade ethanol was obtained from Sigma-Aldrich (Milwaukee, St. Louis, MO, USA).

2.2. BDS Setup and Measurements

In this work, the SURMOF film on borosilicate SiO_2 glass substrates were placed directly on a ground–signal–ground (GSG) coplanar waveguide (CPW) housed in a controlled environment, as we previously described [27]. The 175 mL reactor was purged with a nitrogen–air mixture; a small volume fraction of pure nitrogen was added to the air flow to dilute out any adventitious water vapor in the purging gas while maintaining an aerobic ambient for the inherent oxidation of the analyte. In the bid to prolong the life of the GSG waveguides, all studies were conducted at less than 100 °C, except the initial characterization data shown in Figure 1.

Varying amounts (0.05 to 1 mL) of analytical grade ethanol were injected as needed into the reactor via a long-needled hypodermic syringe, while maintaining the reactor at a preset temperature in an aerobic atmosphere [27].
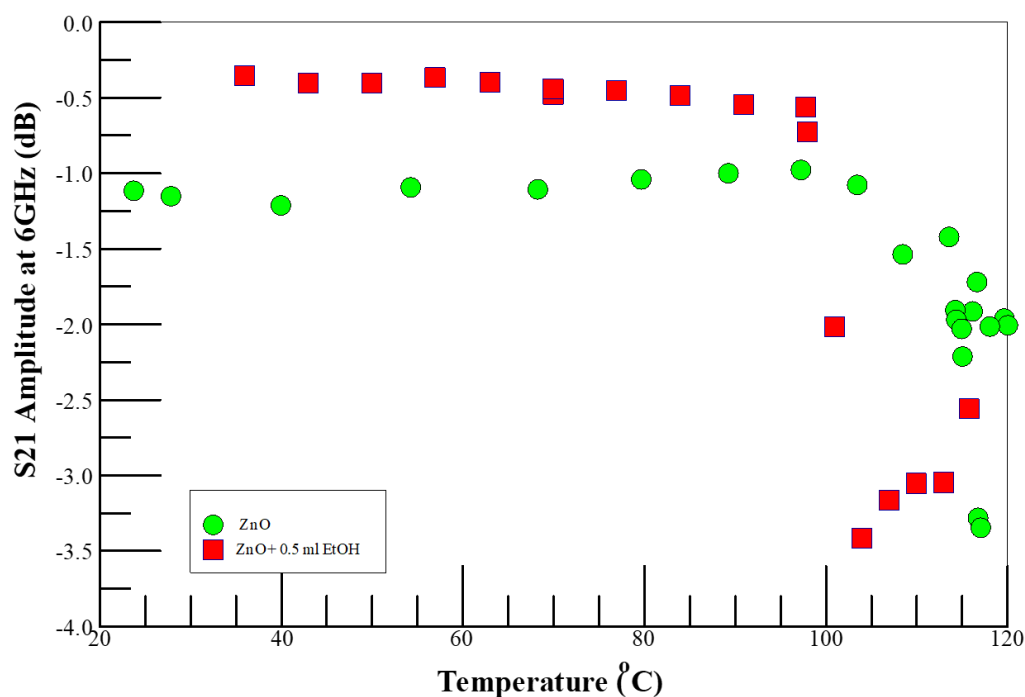
Figure 1. Temperature dependence of microwave insertion loss (S21 amplitude) of ZnO on Si substrate in nitrogen-rich air and gaseous ethanol environments, monitored at 6 GHz. Note that the symbol sizes are much larger than the error bars.

3. Results and Discussion

3.1. BDC Detection of Ethanol Vapor with ZnO Sensors

Chemoresistive metal-oxide-based gas sensors, such as ZnO, rely on conductometric transduction principles [23], i.e., the electrical resistance of the active sensing structure changes in response to redox-active analyte molecules. For n-type ZnO-sensing materials, the gas-sensing mechanism involves perturbing the electron concentration in the conduction band. When the ZnO nanorods are exposed to ethanol vapor in an aerobic ambiance at appropriate temperatures, the alcohol molecule is oxidized to form aldehydes in a three-step charge-transfer process [44]:

(1) The sensor activation step involves the formation of a depletion layer at the air/ZnO-nanorod interface from adsorbed oxygen species on the surface of the ZnO; the speciation of the adsorbed oxygen depends on temperature: O^{2-} at temperatures less than $100\,°C$; O^- at temperatures between 100 and $300\,°C$, and O^{2-} at temperatures higher than $300\,°C$ [2];

(2) Analyte gas molecules adsorb onto the oxygen-rich ZnO nanorod surface to form adducts;

(3) The adducts oxidize/reduce through charge-transfer reactions in the 200–400 °C temperature range; this perturbs the electron density in the conduction band, altering the resistivity of the sensing device.

The number of electrons (i.e., coulombs) released into the conduction band is limited by the number of adsorbed analyte molecules, the surface area, and the chemistry of the surface. It has been demonstrated experimentally that the sensitivity and response speed of VOC detection with ZnO appears to depend on numerous factors, including but not limited to the nanoscale morphology, quality, and chemistry of the ZnO surface. For example, while ZnO microrods on SiO_2/Si substrate synthesized at low temperature (95° C) via wet chemical process showed maximum sensitivity and response time for ethanol and methanol vapor detection at 150 °C [45], we have shown elsewhere that hydrothermally synthesized ZnO nanorods grown on fine-grained random nanocrystalline-seed ZnO layers [39] prepared by atomic layer deposition (ALD) exhibit maximum sensitivity at around 320 °C [38].

Figure 1 shows the temperature dependence of microwave insertion loss (S_{21} amplitude, reported at 6 GHz) of ZnO on Si in nitrogen-enriched air (air–N_2) and in gaseous ethanol environments, respectively, monitored at 6 GHz. While the system impedance (denoted by the insertion-loss amplitude (S_{21} amplitude) was stable below 100 °C, the system impedance increased with increasing temperature above 100 °C, which may be due to the speciation changes during the sensor activation step (i.e., as discussed in step 1 above), and changes in interfacial capacitance that result from the surface potential barrier formed from the adsorption of the analyte species from the environment onto the ZnO [46,47], along with the temperature dependence of the intrinsic semiconductor resistivity properties of the ZnO nanotubes grown on silicon substrate. The contribution of the interfacial capacitance is illustrated by the introduction of ethanol vapor into the reactor, as shown in Figure 1. It is proposed that at temperatures lower than 100 °C, the ethanol molecules adsorb to form adducts with the pre-existing oxygen-adsorbed species. At suitably higher temperatures, the adducts further react. This initial adduct formation alters the electrostatics of the ZnO system, manifesting as increased impedance of the system and higher insertion losses. The BDS response to the ethanol analyte at temperatures less than 100 °C is rather remarkable since there is no conductometric response of ethanol vapor on ZnO nanorods at temperatures below 100 °C [21].

The perturbation of the conductivity of the sensing element is traditionally measured through coulometry; however, each of the elementary processes discussed above involves changes in the surface polarizability, which can be discussed with chemisorption models without specifying the details of the surface reactions and the sensing mechanism [48]. These chemisorbed models are easily monitored by corresponding changes in microwave S-parameters. Using BDS, we previously investigated the three steps discussed above, and showed that ethanol can be detected on our ZnO nanorods at temperatures well below 100 °C [27]. As we discuss below, we observed the formation of ethanol–O_2^- adducts on the ZnO-nanorod surface which do not have to react chemically to change the impedance of the sensor. Thus, the ability to detect chemisorbed species at low temperatures with BDS negates the need for high-temperature charge-transfer reactions to capture the quantity of electrons transferred in to infer the number of adsorbed analyte molecules present.

3.2. Ethanol Vapor Detection with Pristine and TCNQ-loaded HKUST-1 SURMOF

The potential of metal–organic frameworks (MOFs) for gas mixture separation [49], and as VOC-sensing agents have been discussed in the literature [12,14]. Furthermore, copper MOFs are widely used in MOF alcohol oxidation, due to the intrinsic activity of copper as an oxidizing catalyst [50]. The HKUST-1 MOF, $[Cu_3(BTC)_2(H_2O)_3]_n$ (where BTC is benzene-1,3,5-tricarboxylate), is composed of square Cu–Cu paddlewheel clusters connected by BTC ligands to form a rigid porous open framework with bimodal pore size distribution [51,52], and two-coordination unsaturated $Cu[2]^+$ metal sites (open metal sites) per paddlewheel where polar groups can attach through dative bonding [53]. The open metal sites, formed by removing axial ligands, strongly coordinate to electron-rich species (i.e., Lewis bases). The HKUST-1 MOF has three distinct internal pores, two of comparable size (aperture = 14 Å) and a smaller pore (aperture = 10 Å). One of the two larger pores has the Cu–Cu paddlewheels directed into the pores making it suitable for coordinating TCNQ guest molecules. The open metal sites in the smaller pores are still available for coordinating to small molecules [53,54]. The open Cu sites in the small cavities are separated by 8.2 Å, which limits the size, stereochemistry, and the number analyte molecules that could be adsorbed at those sites [50]. Small aliphatic alcohol molecules and similar-sized polar molecules reversibly adsorb at the available open metal centers in the MOF cavity, causing the cavity to expand and inducing changes in its physicochemical properties, such as decreased thermal conductivity [26] and electrical conductivity of the MOF [13,55,56]. Experimental data suggest that charge transfer between the adsorbed analyte and the open metal sites occurs within the pores of the MOF framework [12]. The

adsorption at the metal sites also results in a change in the interfacial polarization and permittivity, which should be readily detected by microwave energy dissipation [57].

Copper MOFs are widely used as catalysts for alcohol oxidation, due to the intrinsic activity of copper as an oxidizing catalyst [50]. For example, Guo et al. demonstrated that mixed-metal CuPd-HKUST-1 MOF exhibits superior catalytic performance compared to the pristine HKUST-1 for the selective aerobic oxidation of benzyl alcohol to benzaldehyde [56]. Defective HKUST-1 thin films [57], such as those used in this work contain Cu^{2+}/Cu^{+} dimers that form reactive adducts with dioxygen molecules, which are probably responsible for the catalytic aerobic oxidative properties of the HKUST-1 MOF [58]. These oxidative abilities of defects are similar to aerobic organisms, such as in respiration [59]. Copper(I)–dioxygen (O_2) adducts have been proposed as intermediates in dioxygen-activating enzymes; they are capable of oxidizing substrates containing weak O–H and C–H bonds. Mechanistic studies for some enzymes and model systems have supported an initial hydrogen-atom abstraction via the cupric-superoxide complex as the first step of substrate oxidation [60,61]. In the rate-determining step, an O-coordinated alcoholate undergoes an H-abstraction reaction from the α-carbon atom of the alcoholate to generate a bound ketyl radical, which is then intramolecularly converted via one-electron oxidation to the aldehyde with the reduction of the Cu (II) center into a Cu-I species, which is then later deoxidized O_2 [62]. Thus, we expect the absorbed alcohol analyte to be aerobically oxidized in the host MOF to the corresponding aldehydes [63]. These redox reactions at the metal centers should be readily detected by BDS, because of the expected changes in the conductivity of the HKUST-1 SURMOF [13]. Furthermore, microwave (MW) irradiation is known to rapidly convert alcohols to carbonyl compounds over transition metal catalysts [64]. MW irradiation of immobilized reactants on inorganic supports reduces the reaction time and promotes the yield, selectivity, and purity of the products, as the microwave irradiation promotes faster and more efficient internal heating through direct interaction between microwave energy and the reactants [65–67].

In analogy to the aerobic oxidation of aliphatic alcohols on ZnO, we propose conceivable elementary steps involved in the BDS detection of aliphatic alcohols in TCNQ-doped HKUST-1 SURMOF. We expect the adsorbed aliphatic alcohol analyte at the open Cu-sites in the host MOF sites to be aerobically oxidized into aldehydes [63] in a process comprising multiple steps, each with its characteristic polarization dynamics, viz.:

(1) Analyte molecules diffuse into size-accessible cavities to coordinate to the available open Cu^{2+} active sites, some of which exist as Cu^{2+}-Cu^{+}-O_2 adducts, in the HKUST-1 MOFs. This induces an impedance increase in the device under test (DUT) due to distortion of the mechanical structure, along with changes in the electronic band structure that lead to changes in the conductivity of the MOF. In a pure nitrogen ambient, the N_2 adsorbs on the metal sites [68], but in the presence of Lewis base molecules, such as aliphatic alcohols, the analyte is expected to displace pre-adsorbed N_2 molecules from the open metal sites.

(2) The aliphatic alcohol probably coordinates to the open metal center via the hydroxyl-oxygen atom. The alcohol analyte is aerobically oxidized by the Cu-sites [69] into carbonyl compounds (e.g., aldehydes from the primary) at room temperature [12], with electrons transferred into the MOF from the alcohol, as discussed above. This step is dependent on the presence of oxygen in the ambient within the reactor, which is required for the reoxidation of the Cu(I) to Cu(II). The resultant carbonyl compounds, because of their increased electrophilic nature, are more polarizable, and contribute to the observed increased insertion loss.

(3) The oxidation of the adsorbed alcohol analyte in the MOF into aldehydes, in step 2, may be aided by the probe microwave stimulus.

There are multiple dielectric mechanisms and polarization processes inherent in the HKUST-1–analyte interactions that can be triggered using different frequencies [70]; thus, careful analyses of the BDS spectra could afford deep mechanistic insights into the VOC

detection as each event results in changes in polarization and has a characteristic relaxation frequency [71].

Nitrogen-enriched air, without ethanol, was used in the initial characterization studies to understand the impact of Lewis base coordination to the open Cu^{2+} centers in the SURMOF films, i.e., to investigate step 1 of the proposed mechanism. Figure 2 shows the temperature dependence of microwave insertion loss (S21 amplitude) in TCNQ-doped HKUST-1 SURMOF in N_2-rich air. The insertion loss is higher in the nitrogen-rich environment than in pure air and increased with increasing temperature from 22 to 40 °C, then leveled off at higher temperatures. Seebeck coefficient measurements indicate holes as the majority charge carriers in TCNQ-HKUST-1 films at room temperature [72], and charge transport is only in the vertical direction in the highly oriented films [40]. The observation of the system becoming more resistive in the nitrogen-enriched air suggests that the N_2 molecules (Lewis base) coordinate to the open Cu^{2+} centers [73] and reduce the concentration of the majority hole carriers [72]. The behavior of the doped material is also consistent with guest-induced electronic and vibrational structure changes of the SURMOF films [26,74]. Furthermore, the temperature dependence of the impedance in the SURMOF suggests that either nitrogen adsorption at the open metal sites is gated by thermal-induced conformational changes in the MOF cage to allow access to the open metal sites [75,76], or the DUT has temperature drifts below 50 °C [77]. Irrespective of the reason for the S_{21} saturation above 50 °C, all subsequent experiments were conducted at 65° C or higher temperatures to avoid the S_{21} drift.
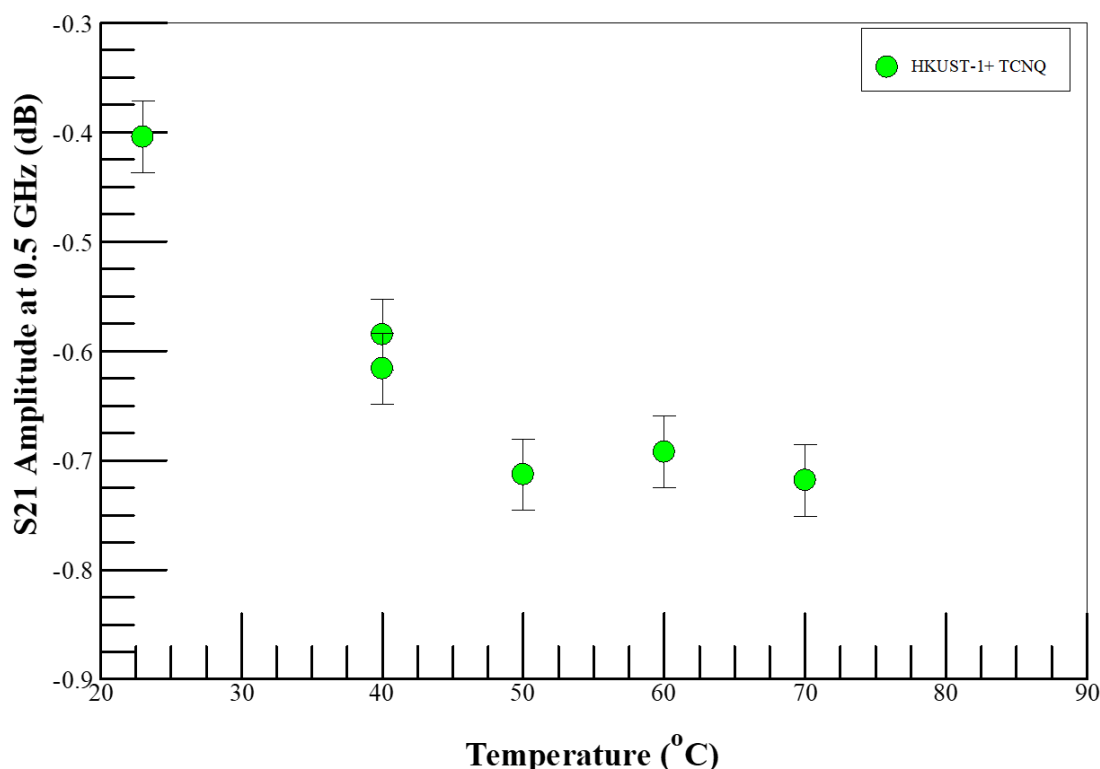

Figure 2. Temperature dependence of microwave insertion loss (S21 amplitude) in TCNQ-loaded HKUST-1 MOF on a Si sample in N_2-rich air. The error bars represent the standard deviation of three or more measurements on the same sample.

Figure 3 shows the S21 amplitude with increasing concentration of the ethanol vapor at a fixed temperature of 80 °C in air. The S21 appears to saturate above 0.5 mL of injected neat ethanol. As in the nitrogen ambient, the system becomes resistive as the methanol (Lewis base) coordinates to the open Cu^{2+} centers [73] and reduces the concentration of the majority hole carriers by donating electrons to the electron-deficient metal site. As

discussed above, holes are the majority carriers in TCNQ-doped HKUST-1 [72], and charge transport is only in the vertical direction in the highly oriented SURMOF films [40], such as those used here. Based on the results from currently ongoing work in our laboratory, we suggest that the ethanol molecules probably coordinate with otherwise free metal centers, and hydrogen bonds to TCNQ dopant, to reduce the hole concentration by electron injection into the SURMOF from the oxidation of the analyte. This explains the increase in the resistance of the system with increasing analyte concentration.
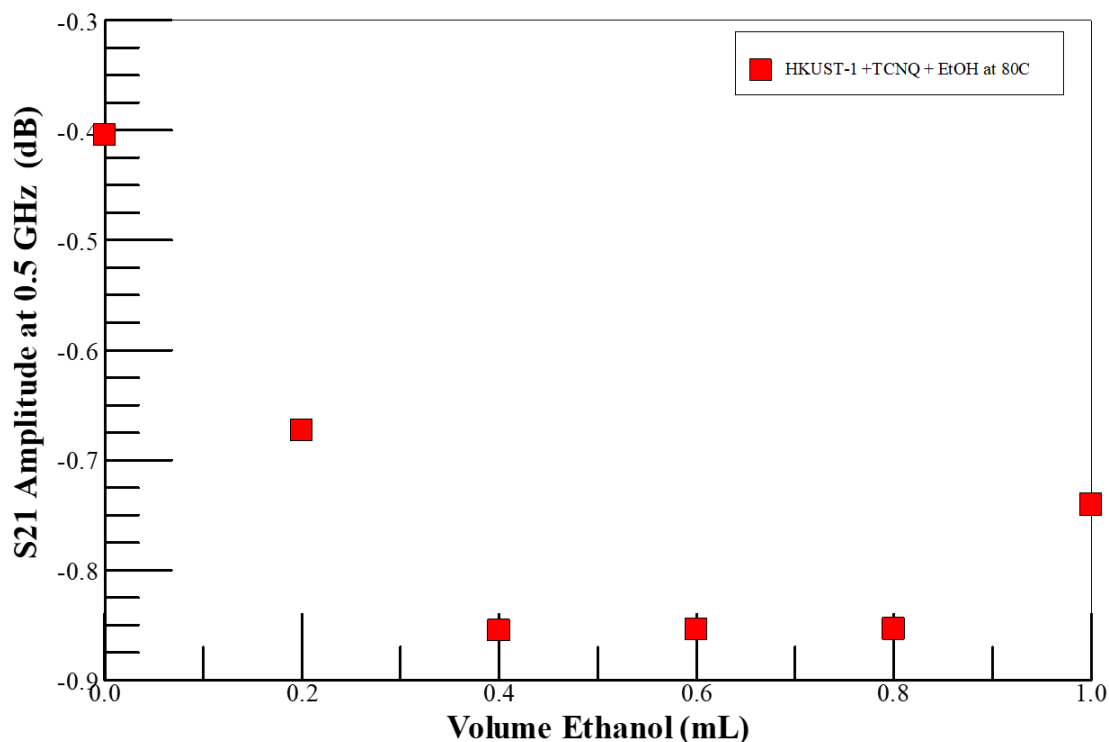

Figure 3. Insertion loss (S21 amplitude) monitored at 0.5 GHz as a function of volume of neat ethanol injected into vapor reactor (i.e., ethanol vapor concentration) environments at 80 C° in air.

It has been demonstrated that only a single layer of adsorbed analyte is formed when the SURMOF layer is exposed to ethanol. The ethanol molecules coordinate to the open Cu centers via the hydroxyl-oxygen atom from the ethanol, and only a single layer is formed due to the weak hydrogen-bonding interactions from coordinated ethanol molecules with additional adsorbed ethanol molecules [78]. Furthermore, the ethanol analyte does not lead to the degradation of the MOF-sensing material. In contrast to water, the ethanol sorption capacity of HKUST-1 remained unchanged with the sorption experiment time, at least at 303 K. In contrast to water, ethanol's weaker interaction with the open Cu(II) sites does not lead to the breaking of the Cu-carboxylate bond in the host HKUST-1 [79]. Thus, the evolution of S21 with ethanol volume, as shown in Figure 3, reflects the adsorption of the analyte into the SURMOF-sensing layer. Up to 0.4 mL (i.e., ~1.1 times the volume of the reactor, or 1.5×10^{13} times the volume of the SURMOF at 80 °C) of ethanol is adsorbed into the SURMOF-sensing layer, which is reminiscent of the adsorption of small molecules into MOF materials [79]. Beyond analyte saturation of the sensing element, additional ethanol volumes do not contribute to the sensor performance; the additional molecules are trapped between the SURMOF substrate and the waveguide or condense on the waveguide end-launch connectors to reduce the system impedance.

3.3. Comparison of BDS Detection of Ethanol on MOF- and ZnO-Sensing Media

Figure 4 compares the microwave insertion loss (S_{21}) dependence on the volume of neat ethanol flash vaporized into the reactor at 80 °C for ZnO to TCNQ-doped HKUST-1 SURMOF in nitrogen-enriched air, monitored at 0.1 GHz. The error bars represent the standard deviation of at least three replicate measurements. In the case of TCNQ-doped MOFs, the charge-transfer reactions inject electrons into the metal center to reduce the hole majority carrier and increase the device resistance. In contrast, ethanol adsorption on ZnO induced relatively small concentration-dependent changes in the device impedance. Thus, the doped HKUST-1 SURMOF films were shown to be more sensitive in detecting ethanol at temperatures below 100 °C than their ZnO analogs. As discussed above, while the ZnO was detected through capacitance changes due to the ethanol-O^{2-} adducts formed on the nanorod's surface, the detection with the MOF is through direct electron injection into the conduction band. Clearly, the MOF system is more sensitive to ethanol concentration than the ethanol detection on ZnO. We admit that 80 °C is substantially below the optimum VOC detection temperature of around 300 °C for ZnO nanorods, but we have shown elsewhere that the BDS can detect a VOC at these low temperatures [27]. Analysis of the BDS data (at specific frequencies) provides electrical information that can be correlated to elementary processes, such as the adduct formation on oxidized ZnO, and charge-transfer reactions in the doped KHUST-1 SURMOF-sensing material [80]. Clearly, the BDS technique affords the capability to distinguish between different impedance-changing mechanisms and provides new mechanistic insights into the elementary events that occur on the ZnO surface during the initial activation step for ethanol detection.
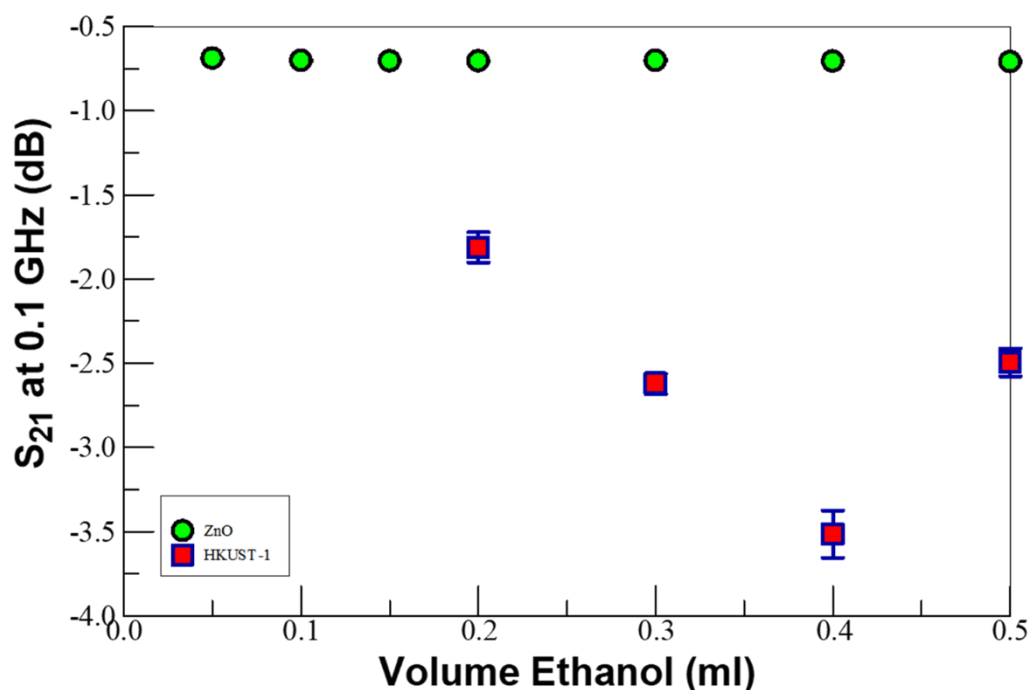

Figure 4. Comparison of the microwave insertion loss (S21) dependence on ethanol concentration on ZnO versus TCNQ-doped-HKUST-1 MOF on Si in gaseous ethanol environments, monitored at 0.1 GHz. Note the error bars represent the standard deviation of at least 3 replicate measurements.

4. Conclusions

Using microwave signal attenuation, we demonstrated physics consistent with analyte-induced physicochemical changes of the sensing media, consistent at a temperature as low as 80 °C on both ZnO- and TCNQ-doped HKUST-1 SURMOF films. In the case of TCNQ-doped HKUST SURMOFs, the charge-transfer reactions inject electrons into the metal center to reduce the hole majority carrier and increase the device resistance. In contrast, ethanol adsorption on ZnO induced relatively small concentration-dependent

changes in the device impedance, mostly through changes in surface electrostatics. The doped HKUST-1 SURMOF films were shown to be more sensitive in detecting ethanol at temperatures below 100 °C than their ZnO analogs. Additionally, the BDS technique affords new mechanistic insights into the elementary events that occur on the ZnO surface during the initial activation step for ethanol detection.

Author Contributions: Sample preparation, methodology, experimentation, data analysis, manuscript writing, P.K.A.; Sample preparation, Z.M.H., P.L.; Sample preparation, supervision, manuscript writing, E.R.; Conceptualization, experimentation, data analysis, manuscript writing, funding, supervision, H.B.; Conceptualization, methodology, experimentation, data analysis, manuscript writing-review, editing, project management, funding, Y.S.O. All authors have read and agreed to the published version of the manuscript.

Institutional Review Board Statement: Not applicable.

Informed Consent Statement: Not applicable.

Data Availability Statement: Data available on request from the authors.

Conflicts of Interest: The authors declare no conflict of interest.

References

1. Korotcenkov, G. *Chemical Sensors: Comprehensive Sensor Technologies Volume 4: Solid State Devices*; Momentum Press: New York, NY, USA, 2011.
2. Meng, F.; Shi, X.; Yuan, Z.; Ji, H.; Qin, W.; Shen, Y.; Xing, C. Detection of four alcohol homologue gases by ZnO gas sensor in dynamic interval temperature modulation mode. *Sens. Actuators B Chem.* **2022**, *350*, 130867. [CrossRef]
3. Korotcenkov, G.; Brinzari, V.; Cho, B.K. Conductometric gas sensors based on metal oxides modified with gold nanoparticles: A review. *Microchim. Acta* **2016**, *183*, 1033–1054. [CrossRef]
4. Dey, A. Semiconductor metal oxide gas sensors: A review. *Mater. Sci. Eng. B* **2018**, *229*, 206–217. [CrossRef]
5. Gopel, W. Chemisorption and charge transfer at ionic semiconductor surfaces: Implications in designing gas sensors. *Prog. Surf. Sci.* **1985**, *20*, 9–103. [CrossRef]
6. Mirzaei, A.; Leonardi, S.G.; Neri, G. Detection of hazardous volatile organic compounds (VOCs) by metal oxide nanostructures-based gas sensors: A review. *Ceram. Int.* **2016**, *42*, 15119–15141. [CrossRef]
7. S. R. Mobasser, J.; Zhang, Y.; Shi, W.; Dittrich, T.M.; Miller, C.J. Internet of things-based edge computing (IoTEC) sensor network and integrated air purifier for rapid response vapor intrusion identification and potential mitigation. In Proceedings of the 2019 Superfund Research Program (SRP) Annual Meeting, Seattle, WA, USA, 18–20 November 2019.
8. Ahn, J.; Kim, H.; Kim, E.; Ko, J. VOCkit: A low-cost IoT sensing platform for volatile organic compound classification. *Ad Hoc Netw.* **2021**, *113*, 102360. [CrossRef]
9. Chowdhury, F.U.M.; Gardner, J. Gardner, Benefits of CMOS Sensors for Environmental Monitoring. In Proceedings of the Fourth Scientific Meeting EuNetAir, Linkoping, Sweden, 3–5 June 2015; pp. 40–43.
10. Nourbakhsh, A.; Yu, L.; Lin, Y.; Hempel, M.; Shiue, R.-J.; Englund, D.; Palacios, T. Heterogeneous Integration of 2D Materials and Devices on a Si Platform. In *Beyond-CMOS Technologies for Next Generation Computer Design*; Topaloglu, R.O., Wong, H.S.P., Eds.; Springer International Publishing: Cham, Switzerland, 2019; pp. 43–84.
11. Shulaker, M.M.; Hills, G.; Park, R.S.; Howe, R.T.; Saraswat, K.; Wong, H.S.P.; Mitra, S. Three-dimensional integration of nanotechnologies for computing and data storage on a single chip. *Nature* **2017**, *547*, 74–78. [CrossRef]
12. Koo, W.-T.; Jang, J.-S.; Kim, I.-D. Metal-organic frameworks for chemiresistive sensors. *Chem* **2019**, *5*, 1938–1963. [CrossRef]
13. Calvo, J.J.; Angel, S.M.; So, M.C. Charge transport in metal–organic frameworks for electronics applications. *APL Mater.* **2020**, *8*, 050901. [CrossRef]
14. Kreno, L.E.; Leong, K.; Farha, O.K.; Allendorf, M.; van Duyne, R.P.; Hupp, J.T. Metal–organic framework materials as chemical sensors. *Chem. Rev.* **2012**, *112*, 1105–1125. [CrossRef]
15. Xu, W.-Q.; He, S.; Lin, C.-C.; Qiu, Y.-X.; Liu, X.-J.; Jiang, T.; Liu, W.-T.; Zhang, X.-L.; Jiang, J.-J. A copper based metal-organic framework: Synthesis, modification and VOCs adsorption. *Inorg. Chem. Commun.* **2018**, *92*, 1–4. [CrossRef]
16. Min, Y. Properties and Sensor Performance of Zinc Oxide Thin Films. Ph.D. Thesis, Massachusetts Institute of Technology, Cambridge, MA, USA, 2003.
17. Homayoonnia, S.; Zeinali, S. Design and fabrication of capacitive nanosensor based on MOF nanoparticles as sensing layer for VOCs detection. *Sens. Actuators B Chem.* **2016**, *237*, 776–786. [CrossRef]
18. Sophocleous, M. Electrical resistivity sensing methods and implications. In *Electrical Resistivity and Conductivity*; InTech: Rijeka, Croatia, 2017.

19. Rydosz, A.; Maciak, E.; Wincza, K.; Gruszczynski, S. Microwave-based sensors with phthalocyanine films for acetone, ethanol and methanol detection. *Sens. Actuators B Chem.* **2016**, *237*, 876–886. [CrossRef]

20. Li, F.; Zheng, Y.; Hua, C.; Jian, J. Gas sensing by microwave transduction: Review of progress and challenges. *Front. Mater.* **2019**, *6*, 101. [CrossRef]

21. Xu, F.; Zhou, C.; Ho, H.-P. A rule for operation temperature selection of a conductometric VOC gas sensor based on ZnO nanotetrapods. *J. Alloys Compd.* **2021**, *858*, 158294. [CrossRef]

22. Lord, A.M.; Maffeis, T.G.; Walton, A.S.; Kepaptsoglou, D.M.; Ramasse, Q.M.; Ward, M.B.; Köble, J.; Wilks, S.P. Factors that determine and limit the resistivity of high-quality individual ZnO nanowires. *Nanotechnology* **2013**, *24*, 435706. [CrossRef] [PubMed]

23. Kim, I.-D.; Rothschild, A.; Tuller, H.L. Advances and new directions in gas-sensing devices. *Acta Mater.* **2013**, *61*, 974–1000. [CrossRef]

24. Müller, K.; Vankova, N.; Schöttner, L.; Heine, T.; Heinke, L. Dissolving uptake-hindering surface defects in metal–organic frameworks. *Chem. Sci.* **2019**, *10*, 153–160. [CrossRef]

25. Babaei, H.; DeCoster, M.E.; Jeong, M.; Hassan, Z.M.; Islamoglu, T.; Baumgart, H.; McGaughey, A.J.H.; Redel, E.; Farha, O.K.; Hopkins, P.E.; et al. Observation of reduced thermal conductivity in a metal-organic framework due to the presence of adsorbates. *Nat. Commun.* **2020**, *11*, 4010. [CrossRef]

26. DeCoster, M.E.; Babaei, H.; Jung, S.S.; Hassan, Z.M.; Gaskins, J.T.; Giri, A.; Tiernan, E.M.; Tomko, J.A.; Baumgart, H.; Norris, P.M.; et al. Hybridization from Guest–Host Interactions Reduces the Thermal Conductivity of Metal–Organic Frameworks. *J. Am. Chem. Soc.* **2022**, *144*, 3603–3613. [CrossRef]

27. Amoah, P.K.; Lin, P.; Baumgart, H.; Franklin, R.; Obeng, Y.S. Broadband dielectric spectroscopic detection of volatile organic compounds with ZnO nanorod gas sensors. *J. Phys. D Appl. Phys.* **2020**, *54*, 135104. [CrossRef] [PubMed]

28. Ulloa, R.Z.; Santiago, M.G.H.; Rueda, V.L.V. The interaction of microwaves with materials of different properties. In *Electromagnetic Fields and Waves*; IntechOpen: London, UK, 2019.

29. Chen, R. First-Principles Study on Electronic and Optical Properties of Copper-Based Chalcogenide Photovoltaic Materials. Ph.D. Thesis, School of Industrial Engineering and Management, Department of Materials, Science and Engineering, KTH Royal Institute of Technology, Stockholm, Sweden, 2017.

30. Ambrosch-Draxl, C.; Sofo, J.O. Linear optical properties of solids within the full-potential linearized augmented planewave method. *Comput. Phys. Commun.* **2006**, *175*, 1–14. [CrossRef]

31. Entesari, K.; Ghiri, R.E.; Kaya, E. Broadband dielectric spectroscopy: Recent developments in microwave time-domain techniques. *IEEE Microw. Mag.* **2021**, *22*, 26–48. [CrossRef]

32. Obeng, Y.S.; Nablo, B.J.; Reyes, D.R.; Poster, D.L.; Postek, M.T. Broadband Dielectric Spectroscopy as a Potential Label-Free Method to Rapidly Verify Ultraviolet-C Radiation Disinfection. *J. Res. Natl. Inst. Stand. Technol.* **2021**, 126. [CrossRef]

33. Lin, P. *Enhanced Sensing Performance of Novel Nanostructured ZnO Gas Sensors in Ethanol Vapor Concentration Detection Applications*; Old Dominion Universit: Norfolk, VA, USA, 2019.

34. Kremer, F.; Schönhals, A. *Broadband Dielectric Spectroscopy*; Springer: Berlin/Heidelberg, Germany, 2003.

35. Marghany, M. (Ed.) *Synthetic Aperture Radar Imaging Mechanism for Oil Spills*; Gulf Professional Publishing: Houston, TX, USA, 2020; pp. 73–92.

36. Wernbacher, A.M.; Eichelbaum, M.; Risse, T.; Cap, S.; Trunschke, A.; Schlögl, R. Operando electrical conductivity and complex permittivity study on vanadia oxidation catalysts. *J. Phys. Chem. C* **2019**, *123*, 8005–8017. [CrossRef]

37. Kim, H.-J.; Lee, J.-H. Highly sensitive and selective gas sensors using p-type oxide semiconductors: Overview. *Sens. Actuators B Chem.* **2014**, *192*, 607–627. [CrossRef]

38. Lin, P.; Chen, X.; Zhang, K.; Baumgart, H. Improved Gas Sensing Performance of ALD AZO 3-D Coated ZnO Nanorods. *ECS J. Solid State Sci. Technol.* **2018**, *7*, Q246–Q252. [CrossRef]

39. Biehler, E.; Whiteman, R.; Lin, P.; Zhang, K.; Baumgart, H.; Abdel-Fattah, T. Controlled Synthesis of ZnO Nanorods Using Different Seed Layers. *ECS J. Solid State Sci. Technol.* **2020**, *9*, 121008. [CrossRef]

40. Chen, X.; Zhang, K.; Hassan, Z.M.; Redel, E.; Baumgart, H. Charge Transport, Conductivity and Seebeck Coefficient in Pristine and TCNQ Loaded Preferentially Grown Metal-Organic Framework Films. *J. Phys. Condens. Matter* **2021**. [CrossRef]

41. Arslan, H.K.; Shekhah, O.; Wohlgemuth, J.; Franzreb, M.; Fischer, R.A.; Wöll, C. High-Throughput Fabrication of Uniform and Homogenous MOF Coatings. *Adv. Funct. Mater.* **2011**, *21*, 4228–4231. [CrossRef]

42. Müller, K.; Fink, K.; Schöttner, L.; Koenig, M.; Heinke, L.; Wöll, C. Defects as Color Centers: The Apparent Color of Metal–Organic Frameworks Containing Cu^{2+}-Based Paddle-Wheel Units. *ACS Appl. Mater. Interfaces* **2017**, *9*, 37463–37467. [CrossRef] [PubMed]

43. Talin, A.A.; Centrone, A.; Ford, A.C.; Foster, M.E.; Stavila, V.; Haney, P.; Kinney, R.A.; Szalai, V.; el Gabaly, F.; Yoon, H.P.; et al. Tunable Electrical Conductivity in Metal-Organic Framework Thin-Film Devices. *Science* **2014**, *343*, 66–69. [CrossRef]

44. Wang, L.; Kang, Y.; Liu, X.; Zhang, S.; Huang, W.; Wang, S. ZnO nanorod gas sensor for ethanol detection. *Sens. Actuators B Chem.* **2012**, *162*, 237–243. [CrossRef]

45. Sinha, M.; Mahapatra, R.; Ghosh, R. Ethanol and methanol gas sensing properties of ZnO microrods. *Mater. Today Proc.* **2019**, *11*, 708–713. [CrossRef]

46. Bejaoui, A.; Guerin, J.; Zapien, J.A.; Aguir, K. Theoretical and experimental study of the response of CuO gas sensor under ozone. *Sens. Actuators B Chem.* **2014**, *190*, 8–15. [CrossRef]

47. Bejaoui, A.; Guerin, J.; Aguir, K. Modeling of a p-type resistive gas sensor in the presence of a reducing gas. *Sens. Actuators B Chem.* **2013**, *181*, 340–347. [CrossRef]

48. Steinhauer, S. Gas sensors based on copper oxide nanomaterials: A review. *Chemosensors* **2021**, *9*, 51. [CrossRef]

49. Ma, D.; Li, Z.; Zhu, J.; Zhou, Y.; Chen, L.; Mai, X.; Liufu, M.; Wu, Y.; Li, Y. Inverse and highly selective separation of CO_2/C_2H_2 on a thulium–organic framework. *J. Mater. Chem. A* **2020**, *8*, 11933–11937. [CrossRef]

50. Dhakshinamoorthy, A.; Asiri, A.M.; Garcia, H. Tuneable nature of metal organic frameworks as heterogeneous solid catalysts for alcohol oxidation. *Chem. Commun.* **2017**, *53*, 10851–10869. [CrossRef]

51. Chui, S.S.-Y.; Lo, S.M.-F.; Charmant, J.P.H.; Orpen, A.G.; Williams, I.D. A Chemically Functionalizable Nanoporous Material $[Cu_3(TMA)_2(H_2O)_3]_n$. *Science* **1999**, *283*, 1148–1150. [CrossRef]

52. Wang, Q.M.; Shen, D.; Bülow, M.; Lau, M.L.; Deng, S.; Fitch, F.R.; Lemcoff, N.O.; Semanscin, J. Metallo-organic molecular sieve for gas separation and purification. *Microporous Mesoporous Mater.* **2002**, *55*, 217–230. [CrossRef]

53. Hendon, C.H.; Walsh, A. Chemical principles underpinning the performance of the metal–organic framework HKUST-1. *Chem. Sci.* **2015**, *6*, 3674–3683. [CrossRef] [PubMed]

54. Dedecker, K.; Dumas, E.; Lavédrine, B.; Steunou, N.; Serre, C. Metal-organic frameworks for the capture of volatile organic compounds and toxic chemicals. In *Metal-Organic Frameworks (MOFs) for Environmental Applications*; Ghosh, S.K., Ed.; Elsevier: Amsterdam, The Netherlands, 2019; pp. 141–178.

55. Guo, P.; Froese, C.; Fu, Q.; Chen, Y.-T.; Peng, B.; Kleist, W.; Fischer, R.A.; Muhler, M.; Wang, Y. CuPd mixed-metal HKUST-1 as a catalyst for aerobic alcohol oxidation. *J. Phys. Chem. C* **2018**, *122*, 21433–21440. [CrossRef]

56. Heinke, L.; Wöll, C. Surface-Mounted Metal-Organic Frameworks: Crystalline and Porous Molecular Assemblies for Fundamental Insights and Advanced Applications. *Adv. Mater.* **2019**, *31*, 1806324. [CrossRef]

57. Sachdeva, S.; Koper, S.J.H.; Sabetghadam, A.; Soccol, D.; Gravesteijn, D.J.; Kapteijn, F.; Sudhölter, E.J.R.; Gascon, J.; de Smet, L.C.P.M. Gas phase sensing of alcohols by Metal Organic Framework–polymer composite materials. *ACS Appl. Mater. Interfaces* **2017**, *9*, 24926–24935. [CrossRef]

58. Wang, W.; Sharapa, D.I.; Chandresh, A.; Nefedov, A.; Heißler, S.; Heinke, L.; Studt, F.; Wang, Y.; Wöll, C. Interplay of Electronic and Steric Effects to Yield Low-Temperature CO Oxidation at Metal Single Sites in Defect-Engineered HKUST-1. *Angew. Chem. Int. Ed.* **2020**, *59*, 10514–10518. [CrossRef]

59. Ho, R.Y.N.; Liebman, J.F.; Valentine, J.S. Biological reactions of dioxygen: An introduction. In *Active Oxygen in Biochemistry*; Valentine, J.S., Foote, C.S., Greenberg, A., Liebman, J.F., Eds.; Springer: Dordrecht, The Netherlands, 1995; pp. 1–36.

60. Shearer, J.; Zhang, C.X.; Zakharov, L.N.; Rheingold, A.L.; Karlin, K.D. Substrate Oxidation by Copper− Dioxygen Adducts: Mechanistic Considerations. *J. Am. Chem. Soc.* **2005**, *127*, 5469–5483. [CrossRef]

61. Quist, D.A.; Diaz, D.E.; Liu, J.J.; Karlin, K.D. Activation of dioxygen by copper metalloproteins and insights from model complexes. *JBIC J. Biol. Inorg. Chem.* **2017**, *22*, 253–288. [CrossRef]

62. Chaudhuri, P.; Hess, M.; Müller, J.; Hildenbrand, K.; Bill, E.; Weyhermüller, T.; Wieghardt, K. Aerobic Oxidation of Primary Alcohols (Including Methanol) by Copper(II)− and Zinc(II)−Phenoxyl Radical Catalysts. *J. Am. Chem. Soc.* **1999**, *121*, 9599–9610. [CrossRef]

63. Silva, T.F.S.; Martins, L.M.D.R.S. Recent advances in copper catalyzed alcohol oxidation in homogeneous medium. *Molecules* **2020**, *25*, 748. [CrossRef]

64. Maes, B.; Marimuthu, T.; Alapour, S.; Friedrich, H.B. Microwave-assisted oxidation reaction of primary alcohols with sensitive functional groups to aldehydes using ruthenium diphosphorus complexes. *Arkivoc* **2020**, 120–135.

65. Sutradhar, M.; Alegria, E.C.B.A.; Barman, T.R.; da Silva, M.F.C.G.; Liu, C.-M.; Pombeiro, A.J.L. 1D copper (II)-aroylhydrazone coordination polymers: Magnetic properties and microwave assisted oxidation of a secondary alcohol. *Front. Chem.* **2020**, *8*, 157. [CrossRef] [PubMed]

66. Hazra, S.; Martins, L.M.D.R.S.; da Silva, M.F.C.G.; Pombeiro, A.J.L. Sulfonated Schiff base copper (II) complexes as efficient and selective catalysts in alcohol oxidation: Syntheses and crystal structures. *RSC Adv.* **2015**, *5*, 90079–90088. [CrossRef]

67. Polshettiwar, V.; Varma, R.S. Microwave-assisted organic synthesis and transformations using benign reaction media. *Acc. Chem. Res.* **2008**, *41*, 629–639. [CrossRef]

68. Bordiga, S.; Regli, L.; Bonino, F.; Groppo, E.; Lamberti, C.; Xiao, B.; Wheatley, P.S.; Morris, R.E.; Zecchina, A. Adsorption properties of HKUST-1 toward hydrogen and other small molecules monitored by IR. *Phys. Chem. Chem. Phys.* **2007**, *9*, 2676–2685. [CrossRef]

69. Rubio-Giménez, V.; Almora-Barrios, N.; Escorcia-Ariza, G.; Galbiati, M.; Sessolo, M.; Tatay, S.; Martí-Gastaldo, C. Origin of the chemiresistive response of ultrathin films of conductive metal–organic frameworks. *Angew. Chem. Int. Ed.* **2018**, *57*, 15086–15090. [CrossRef]

70. Babal, A.S.; Donà, L.; Ryder, M.R.; Titov, K.; Chaudhari, A.K.; Zeng, Z.; Kelley, C.S.; Frogley, M.D.; Cinque, G.; Civalleri, B.; et al. Impact of pressure and temperature on the broadband dielectric response of the HKUST-1 metal–organic framework. *J. Phys. Chem. C* **2019**, *123*, 29427–29435. [CrossRef]

71. Bottreau, A.M.; Dutuit, Y.; Moreau, J. On a multiple reflection time domain method in dielectric spectroscopy: Application to the study of some normal primary alcohols. *J. Chem. Phys.* **1977**, *66*, 3331–3336. [CrossRef]

72. Erickson, K.J.; Léonard, F.; Stavila, V.; Foster, M.E.; Spataru, C.D.; Jones, R.E.; Foley, B.M.; Hopkins, P.E.; Allendorf, M.D.; Talin, A.A. Thin film thermoelectric metal–organic framework with high Seebeck coefficient and low thermal conductivity. *Adv. Mater.* **2015**, *27*, 3453–3459. [CrossRef]

73. Strauss, I.; Mundstock, A.; Treger, M.; Lange, K.; Hwang, S.; Chmelik, C.; Rusch, P.; Bigall, N.C.; Pichler, T.; Shiozawa, H.; et al. Metal–organic framework Co-MOF-74-based host–guest composites for resistive gas sensing. *ACS Appl. Mater. Interfaces* **2019**, *11*, 14175–14181. [CrossRef]

74. Liu, J.; Wächter, T.; Irmler, A.; Weidler, P.G.; Gliemann, H.; Pauly, F.; Mugnaini, V.; Zharnikov, M.; Wöll, C. Electric Transport Properties of Surface-Anchored Metal–Organic Frameworks and the Effect of Ferrocene Loading. *ACS Appl. Mater. Interfaces* **2015**, *7*, 9824–9830. [CrossRef] [PubMed]

75. Janczak, J.; Prochowicz, D.; Lewiński, J.; Fairen-Jimenez, D.; Bereta, T.; Lisowski, J. Trinuclear Cage-Like Zn^{II} Macrocyclic Complexes: Enantiomeric Recognition and Gas Adsorption Properties. *Chem. Eur. J.* **2016**, *22*, 598–609. [CrossRef] [PubMed]

76. Deegan, M.M.; Dworzak, M.R.; Gosselin, A.J.; Korman, K.J.; Bloch, E.D. Gas storage in porous molecular materials. *Chem. Eur. J.* **2021**, *27*, 4531–4547. [CrossRef] [PubMed]

77. Collier-Oxandale, A.M.; Thorson, J.; Halliday, H.; Milford, J.; Hannigan, M. Understanding the ability of low-cost MOx sensors to quantify ambient VOCs. *Atmos. Meas. Tech.* **2019**, *12*, 1441–1460. [CrossRef]

78. Jeong, N.C.; Samanta, B.; Lee, C.Y.; Farha, O.K.; Hupp, J.T. Coordination-Chemistry Control of Proton Conductivity in the Iconic Metal-Organic Framework Material, HKUST-1. *J. Am. Chem. Soc.* **2012**, *134*, 51–54. [CrossRef]

79. Álvarez, J.R.; Sánchez-González, E.; Pérez, E.; Schneider-Revueltas, E.; Martínez, A.; Tejeda-Cruz, A.; Islas-Jácome, A.; González-Zamora, E.; Ibarra, I.A. Structure stability of HKUST-1 towards water and ethanol and their effect on its CO_2 capture properties. *Dalton Trans.* **2017**, *46*, 9192–9200. [CrossRef]

80. Serghei, A.; Sangoro, J.R.; Kremer, F. Broadband Dielectric Spectroscopy on Electrode Polarization and Its Scaling. In *Electrical Phenomena at Interfaces and Biointerfaces*; Wiley: Hoboken, NJ, USA, 2012; pp. 241–273.